Journal of
Materials Chemistry C

PAPER

View Article Online
View Journal | View Issue

Cite this: J. Mater. Chem. C, 2017, 5, 11824

Received 9th September 2017,
Accepted 24th October 2017

DOI: 10.1039/c7tc04130f

rsc.li/materials-c

Magnetic light and forbidden photochemistry: the case of singlet oxygen†

Alejandro Manjavacas, *[a] Roberto Fenollosa,[b] Isabelle Rodriguez, [b]
M. Consuelo Jiménez, [c] Miguel A. Miranda[c] and Francisco Meseguer*[b]

Most optical processes occurring in nature are based on the well-known selection rules for optical transitions between electronic levels of atoms, molecules, and solids. Since in most situations the magnetic component of light has a negligible contribution, the dipolar electric approximation is generally assumed. However, this traditional understanding is challenged by nanostructured materials, which interact strongly with light and produce very large enhancements of the magnetic field in their surroundings. Here we report on the magnetic response of different metallic nanostructures and their influence on the spectroscopy of molecular oxygen, a paradigmatic example of dipole-forbidden optical transitions in photochemistry.

Science and technological applications based on photochemical processes are restricted to those situations involving states of matter that are accessible through light excitation.[1] From a theoretical point of view, photochemical processes are governed by the light–matter interaction Hamiltonian, which, for material systems with subwavelength dimensions such as chemical species (*i.e.*, atoms, molecules, *etc.*), can be conveniently written using a multipolar expansion of the electric and magnetic fields[2,3]

$$\mathcal{H} = -\mathbf{p}\cdot\mathbf{E} - \mathbf{m}\cdot\mathbf{B} - \mathbf{Q}:\nabla\mathbf{E} + \ldots \qquad (1)$$

The first term of this expansion involves the electric dipole moment, **p**, of the chemical species and, consequently, is known as electric dipole (ED) term. In a similar way, the second and the third terms contain the magnetic dipole, **m**, and the electric quadrupole, **Q**, moments, and therefore are known as the magnetic dipole (MD), and electric quadrupole (EQ) terms, respectively. Each of these terms presents specific selection rules that control the conditions under which the associated optical transitions can occur.[3] Usually, the electric component of an electromagnetic field is much larger than the magnetic one. For instance, for a plane wave, their ratio is $E/B = c$, where c is the speed of light. As a consequence of this, most optical processes in light–matter interaction are dominated by dipolar electric transitions.[3]

The situation is completely different when the chemical species undergoing the optical transition is placed near a metallic nanostructure. These systems are well known to support coherent oscillations of their conduction electrons, commonly known as surface plasmons, that couple strongly with light and generate large electromagnetic fields around them.[4,5] Such extraordinary properties have already been exploited in different research areas including biosensing,[6–8] photovoltaics,[9–11] and photocatalysis,[12–14] to cite some. Interestingly, the enhancement of the electromagnetic field produced by these nanostructures comes associated with a strong magnetic response[15–19] that changes dramatically the usual light–matter interaction, thus enabling new amazing phenomena such as negative refraction,[20–22] perfect lensing,[23] or even optical cloaking.[24] To this end, different structures fabricated using top-down[15,25–28] or bottom-up[29–32] techniques have been explored. These include, for instance, metallic split-ring resonators[25] and cut-wire pairs,[26,27] whose magnetic response in the optical region[33,34] has been characterized both at the single particle level[35,36] and for ordered arrays.[15,16,25–27] It is worth to note that high-refractive nanostructures can also produce strong magnetic fields, which are, in this case, associated with photonic cavity modes supported by these systems.[37–43]

The strong magnetic field produced by metallic nanostructures can be used to enhance the MD transitions of chemical species placed in their vicinity (see ref. 44 for a comprehensive review). Such possibility has been theoretically explored[45–47] and experimentally verified using principally rare-earth ions, which exhibit strong MD in the optical range associated with their 4f orbitals,[48–50] placed in closed proximity to plasmonic structures with different designs.[51–59] It is important to note that the

---

[a] *Department of Physics and Astronomy, University of New Mexico, Albuquerque, New Mexico 87131, USA. E-mail: manjavacas@unm.edu*

[b] *Instituto de Tecnología Química (CSIC-UPV), Universitat Politècnica de Valencia, Av. Tarongers s/n, 46022, Valencia, Spain. E-mail: fmese@fis.upv.es*

[c] *Departamento de Química, Universitat Politècnica de Valencia, Av. Tarongers s/n, 46022, Valencia, Spain*

† Electronic supplementary information (ESI) available: Figure summarizing different chemical reactions of interest for detecting and monitoring singlet oxygen formation. See DOI: 10.1039/c7tc04130f

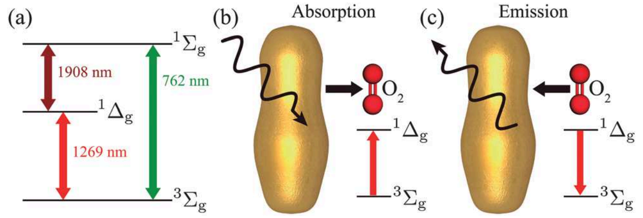

Fig. 1 (a) Relevant energy levels of molecular oxygen. (b and c) Schematics of the two optical processes that can be enhanced by the presence of a resonant metallic nanostructure: (b) an oxygen molecule absorbs a photon and is excited from the $^3\Sigma_g$ to the $^1\Delta_g$ level, (c) an excited oxygen molecule emits a photon and decays from $^1\Delta_g$ to $^3\Sigma_g$. In (b), the absorption probability is increased by the strong enhancement of the magnetic field produced by the metallic nanostructure, while in (c), the emission probability is amplified by the large scattering cross-section of the metallic nanostructure.

strong magnetic field enhancement produced by plasmonic nanostructures in their surroundings normally comes together with an even stronger amplification of its electric counterpart,[60] which enhances the ED transitions of the chemical species. This can be very relevant for species having MD and ED transitions closely located in the spectrum, since, in these cases, the ED transition can obscure the MD transition.[61] A similar effect is expected for EQ transitions, which are enhanced by the large electric field gradients (see eqn (1)) produced near plasmonic nanostructures.[62–66]

Among the many different chemical species that could benefit from the enhancement of the MD optical transitions provided by surface plasmons, molecular oxygen, O_2, constitutes a very relevant example. This molecule is a key specie in nature and, despite its apparent simplicity, exhibits a number of rather unusual properties that strongly influence its spectroscopic behavior, as well as its chemical reactivity.[67] As shown in Fig. 1(a), O_2 has a triplet multiplicity ground state, $^3\Sigma_g$. Conversely, its lowest lying excited states, $^1\Delta_g$ and $^1\Sigma_g$, are of singlet nature and appear at relatively low energies above the ground state. Therefore, due to spin conservation, any transition between the ground $^3\Sigma_g$ and the excited states $^1\Delta_g$ and $^1\Sigma_g$ of O_2 cannot involve the ED and the EQ terms appearing in eqn (1).[68] Only the MD term, which is proportional to the magnetic field, can connect these levels. Such transitions are commonly referred to as forbidden optical transitions. Interestingly, their forbidden nature prevents the spontaneous photo-oxidation of living systems upon exposure to natural sunlight in an aerobic atmosphere. On the other hand, singlet O_2 is not just a relevant model for fundamental chemical and physical phenomena; it also has important applications in fields ranging from atmospheric chemistry and material science to biology and medicine, including photodynamic therapy (PDT) of cancer.[67,69] Singlet molecular oxygen exhibits a unique reactivity as synthetic reagent, as intermediate in oxygenation reactions of polymers, and as part of reactive oxygen species in a range of biological systems.[70]

Usually, the optical activation of O_2, *i.e.*, its transition from the triplet to the singlet state, is achieved through the electronic excitation of photosensitizers, typically visible light-absorbing aromatic compounds with a high intersystem crossing quantum yield.[71] The collected triplet energy is then transferred to molecular oxygen, affording the $^1\Delta_g$ and/or $^1\Sigma_g$ excited states of molecular oxygen.[72,73] Direct optical excitation is very challenging, as demonstrated by the orders of magnitude of the Einstein coefficients for spontaneous emission from the singlet states, which in the gas phase are 10^{-3} s^{-1}, 10^{-1} s^{-1}, and 10^{-4} s^{-1}, for the $^1\Sigma_g \rightarrow {}^1\Delta_g$, $^1\Sigma_g \rightarrow {}^3\Sigma_g$, and $^1\Delta_g \rightarrow {}^3\Sigma_g$ transitions, respectively, while for O_2 dissolved in a liquid such as water, they increase to 10^3 s^{-1}, 10^0 s^{-1}, and 10^{-1} s^{-1}, respectively.[67] These numbers clearly make the excitation and deexcitation of singlet O_2 ideal optical processes that can benefit from the plasmonic enhancement of MD transitions.

In this paper, we investigate the enhancement of the magnetic dipole transitions connecting the triplet $^3\Sigma_g$ and singlet state $^1\Delta_g$ of O_2 in the presence of different metallic nanostructures. Despite the variety of optimized structures already characterized in literature, including split-ring resonators[46] and diabolo structures,[47,74] here we choose to work with single and tip-to-tip welded gold nanorods.[75] The reason for our choice is that, in spite of their simplicity, these structures produce large magnetic field enhancements over a large volume around them, with peak values close to those of optimized nanostructures, but, as opposed to those, can be efficiently synthesized using colloidal chemistry and used in liquid suspension (customarily water), thus providing a larger region for interaction with O_2 than surface patterned nanostructures.[76] This is of vital importance to maximizing the enhancement of photochemical processes as the one investigated here. Using rigorous solutions of Maxwell's equations, we analyze the impact of these structures both in the excitation and deexcitation processes involving singlet O_2, and we discuss different potential experiments for testing the generation and detection of singlet oxygen.

Results

The two different optical processes that we consider in this work are described in Fig. 1(b and c). The first case corresponds to the excitation of O_2 from the $^3\Sigma_g$ to the $^1\Delta_g$ excited state by absorption of a photon. To this end, both the metallic nanostructure and the O_2 molecule are illuminated with an external light source of energy $\hbar\omega$, resonant with the transition wavelength $\lambda_0 = 1269$ nm. The probability per unit time of inducing a transition can be calculated using Fermi's golden rule[3]

$$P = \frac{2\pi}{\hbar^2}\sum_{\mathrm{f}} |\langle \mathrm{f}|\mathcal{H}|\mathrm{i}\rangle|^2 \delta(\omega_{\mathrm{i}} - \omega_{\mathrm{f}}),$$

where $|\mathrm{i}\rangle$ and $|\mathrm{f}\rangle$ are the initial and final states, and $\mathcal{H}$ is the Hamiltonian connecting them. In our case, since the transition is forbidden, the only relevant term of the Hamiltonian given in eqn (1) is the MD, and therefore the probability per unit time of absorption is proportional to $|\mathbf{m}\cdot\mathbf{B}(\mathbf{r}_0)|^2$. Consequently, the increase of this quantity due to the presence of the metallic nanoparticle is given by

$$\frac{P_{\mathrm{a}}}{P_{\mathrm{a}}^{0}}=\left|\frac{\mathbf{B}(\mathbf{r}_0)}{\mathbf{B}_0(\mathbf{r}_0)}\right|^2,$$

and therefore is determined by the enhancement of the magnetic field intensity at the position of the O_2 molecule produced by the plasmonic resonances supported by the metallic nanoparticle. To reproduce an experimental situation, this expression has to be averaged over all possible relative orientations between the external illumination, the metallic nanostructure, and the molecule transition dipole.

The second process considered here corresponds to the spontaneous deexcitation of O_2 from the singlet $^1\Delta_g$ state to the triplet $^3\Sigma_g$ ground state, which is sketched in Fig. 1(c). In this case, the enhancement of the transition probability relative to free space can be written as[77,78]

$$\frac{P_{\mathrm{e}}}{P_{\mathrm{e}}^{0}}=-\frac{2\pi c^3}{\omega}\mathrm{Im}\{\mathrm{Tr}\mathcal{G}(\mathbf{r}_0,\mathbf{r}_0)\},\tag{2}$$

where $\mathcal{G}(\mathbf{r},\mathbf{r}')$ is the magnetic Green's tensor of Maxwell's equations,[79] defined as the solution of

$$\nabla\times\nabla\times\mathcal{G}(\mathbf{r},\mathbf{r}')-\varepsilon(\mathbf{r})\frac{\omega^2}{c^2}\mathcal{G}(\mathbf{r},\mathbf{r}')=-\frac{1}{c^2}\delta(\mathbf{r}-\mathbf{r}'),$$

with the appropriate boundary conditions. It corresponds to the magnetic field produced at $\mathbf{r}$ by a magnetic dipole placed at $\mathbf{r}'$ in the presence of the metallic nanostructure. The symbol Tr in eqn (2) indicates the trace over $\mathcal{G}(\mathbf{r},\mathbf{r})$ necessary to average over all possible dipole orientations. In absence of the metallic nanostructure, P_{e} reduces to P_{e}^{0}, which is the Einstein coefficient for spontaneous emission of the $^1\Delta_g \rightarrow {}^3\Sigma_g$ transition.[79] The enhancement of the emission probability produced by the nanoparticle takes place through two different channels: radiative and nonradiative. In the first case, the nanoparticle acts as an antenna and helps to radiate the photon produced in the deexcitation of O_2. In the second situation, the nanoparticle also enhances the deexcitation process, however, in this case, the generated photon is absorbed by the nanoparticle. Since we are interested in the detection of singlet O_2 through the measurement of the emitted photons, *i.e.*, the photoluminescence, we want to enhance only the first of these two channels. Therefore, we can separate the Green's tensor into two terms: one associated with the radiative channel and the other one corresponding to the nonradiative decay: $\mathcal{G}(\mathbf{r},\mathbf{r}')=\mathcal{G}_{\mathrm{r}}(\mathbf{r},\mathbf{r}')+\mathcal{G}_{\mathrm{nr}}(\mathbf{r},\mathbf{r}')$. This allows us to write an expression for the photoluminescence enhancement due to the metallic nanostructure

$$\frac{P_{\mathrm{e,r}}}{P_{\mathrm{e}}^{0}}=-\frac{2\pi c^3}{\omega}\mathrm{Im}\{\mathrm{Tr}\mathcal{G}_{\mathrm{r}}(\mathbf{r}_0,\mathbf{r}_0)\}.\tag{3}$$

The photoluminescence enhancement can be directly obtained from the calculation of the far-field emission of a classical magnetic dipole in presence and in absence of the nanostructure.

In the following, we investigate the enhancement of the absorption and emission processes associated with the singlet O_2 molecule produced by metallic nanostructures. In particular, we focus on two different systems, namely a pair of tip-to-tip welded nanorods and a single nanorod. The geometry of the first structure is similar to that of the systems traditionally considered to achieve large enhancement of the magnetic field, usually consisting of two identical nanostructures connected by a narrow junction.[47,74] On the other hand, the single nanorod represents a simpler geometry and consequently involves a less demanding synthesis. In both cases, the dimensions of the nanostructure are chosen to ensure they support a plasmon resonant with the $^1\Delta_g \rightarrow {}^3\Sigma_g$ transition wavelength $\lambda_0 = 1269$ nm. Fig. 2 shows the results obtained for the tip-to-tip welded nanorods. The dimensions of the nanostructure are specified in panel (a); each individual nanorod consists of a cylinder of 49 nm of length and a diameter of 20 nm terminated by two hemispheres of radius 10 nm. The two rods are welded together resulting in a structure with a total length of 136 nm. All the results discussed in the following are obtained by rigorously solving Maxwell's equations using the boundary element method (BEM).[80,81] The dielectric function for gold is taken from tabulated

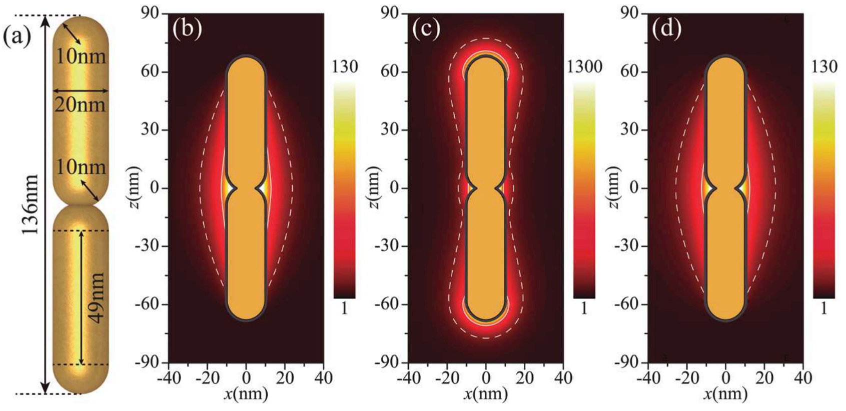

Fig. 2 Optical response of a pair of tip-to-tip welded gold nanorods. (a) Geometry of the nanostructure. (b) Magnetic field intensity enhancement $|\mathbf{B}|^2/|\mathbf{B}_0|^2$ averaged over all possible light incidence directions and polarizations. (c) Electric field intensity enhancement $|\mathbf{E}|^2/|\mathbf{E}_0|^2$ averaged over all possible light incidence directions and polarizations. (d) Photoluminescence enhancement $P_{\mathrm{e,r}}/P_{\mathrm{e}}^{0}$. The dashed and solid white contours signal the regions for which the enhancement is larger than 10 and 50 for panels (b) and (d), and larger than 100 and 500 for panel (c). All calculations are performed at λ_0 = 1269 nm.

data,[82] and the nanostructures are assumed to be surrounded by water ($\varepsilon = 1.77$). We restrict the calculations to points separated by at least 0.5 nm from the surface of the structure. The reason is that classical calculations for points located closer to the surface are nonphysical, due to nonlocal effects. Furthermore, this distance also corresponds to the typical size of molecules like cetyltrimethylammonium bromide (CTAB) that are customarily used for obtaining high aspect ratio gold nanorods and stabilizing them in aqueous suspensions.[83,84]

Upon illumination, the nanorod pair generates a strong electromagnetic field around it. Fig. 2(b) shows the magnetic field intensity enhancement $|\mathbf{B}|^2/|\mathbf{B}_0|^2$ produced by this structure, averaged over all possible incidence angles and polarizations. This enhancement can be intuitively understood by noticing that the electron oscillation associated with the longitudinal plasmon supported by the metallic nanostructure produces an electric current that, by virtue of Ampère–Maxwell's law, generates the magnetic field. The narrowing of the structure at its central region produces an increase of the current density, and therefore an even higher enhancement of the magnetic field that can reach values above 100 near the contact point between the nanorods, and, as expected, decays as we move away from that region. The dashed and solid white curves indicate the regions for which the enhancement is above 10 and 50, respectively. Although here we are interested in the magnetic field enhancement, it is important to analyze the response of the electric field, and, in particular, its gradient since, for instance, the transition $^1\Delta_g \rightarrow {}^1\Sigma_g$, which has resonant wavelength $\lambda_0 = 1908$ nm, is EQ allowed. Not surprisingly, the electric field is strongly enhanced near the nanostructure. In particular, as shown in Fig. 2(c), $|\mathbf{E}|^2/|\mathbf{E}_0|^2$ can reach values above 1000, both at the contact region and at the ends of the nanorods. The dashed and solid white curves indicate, in this case, the region for which the enhancement is above 100 and 500, respectively.

The increase in the photoluminescence produced by this nanostructure is studied in Fig. 2(d), where we plot the results obtained with eqn (3) for the tip-to-tip welded nanorods of panel (a). Examining these results, we observe that both the enhancement values and the spatial distribution are similar to those of the magnetic field intensity shown in panel (b). In particular, there is a significant volume around the particle for which the enhancement of the emission probability is above 10 (dashed white curve), while closer to the contact region, these values increase above 50 (solid white curves). These results are coherent with the smaller quenching near metallic structures expected for magnetic transitions as compared with their electric counterparts.[85]

Fig. 3 is devoted to the analysis of the different enhancements associated with the second geometry under consideration, namely a single nanorod, whose synthesis is more direct. As shown in panel (a), the total length of this nanostructure including the hemispheres at the ends is 156 nm, while the diameter is again 20 nm. Such dimensions are chosen to ensure the existence of a plasmon resonance at 1269 nm. Examining panel (b), we observe that the single nanorod produces similar peak values for the magnetic field intensity enhancement as the tip-to-tip welded nanorods, however this enhancement is extended over a larger volume, as inferred from the comparison of the regions enclosed by the dashed and solid white curves of Fig. 2(b) and 3(b). A similar behavior is obtained for the electric field (*cf.* Fig. 3(c)), whose extrema, in this case, appear only at the ends of the nanostructure. Regarding the enhancement of the photoluminescence, as shown in panel (d), it reaches values very similar to those displayed by the tip-to-tip welded nanorods of Fig. 2, but extended over a larger region around the nanostructure. It is important to remark that the enhancement values provided by the structures studied here are not far from those reported for optimized planar geometries, such as diabolo nanostructures, once one takes into account the averaging over all possible relative orientations between the dipole and the nanostructure,[47] but with the advantage that both the single and tip-to-tip welded nanorods can be efficiently synthesized using colloidal chemistry techniques and used in liquid suspension, thus enabling much larger interaction volumes with O_2.

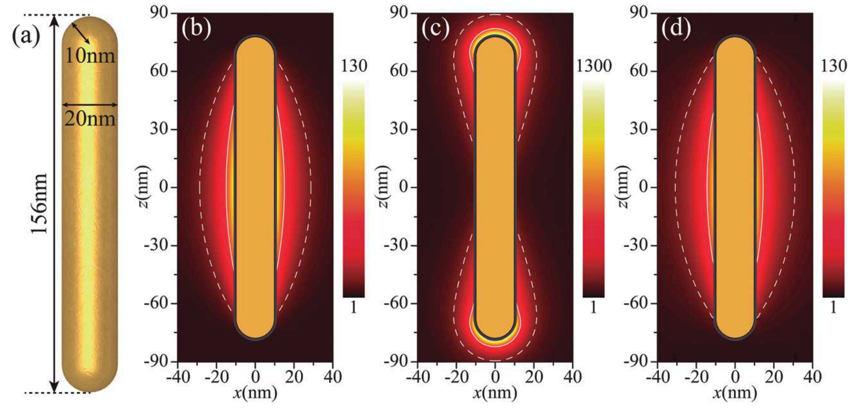

Fig. 3 Optical response of a single gold nanorod. (a) Geometry of the nanostructure. (b) Magnetic field intensity enhancement $|\mathbf{B}|^2/|\mathbf{B}_0|^2$ averaged over all possible light incidence directions and polarizations. (c) Electric field intensity enhancement $|\mathbf{E}|^2/|\mathbf{E}_0|^2$ averaged over all possible light incidence directions and polarizations. (d) Photoluminescence enhancement $P_{e,r}/P_e^0$. The dashed and solid white contours signal the regions for which the enhancement is larger than 10 and 50 for panels (b) and (d), and larger than 100 and 500 for panel (c). All calculations are performed at $\lambda_0 = 1269$ nm.

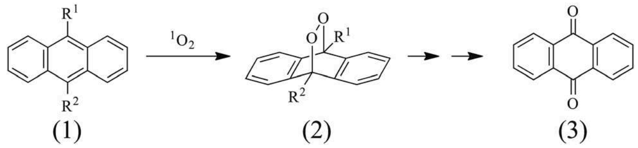

Fig. 4 General reactivity of 9,10-disubstituted anthracenes (1) with formation of an endoperoxide (2) upon addition of singlet oxygen, and rearrangement into an anthraquinone derivative (3).

In the following part, we discuss the potential photochemical reactions that we can carry out for sensing the generation of singlet oxygen in the presence of gold nanorods.

Discussion of the potential photochemical reactions

The formation of singlet O_2 can be monitored by steady state and time-resolved absorption and/or emission measurements, as well as by chemical trapping using selected probes we describe hereafter, or even through quartz-enhanced photoacoustic spectroscopy.[86] As the photoactivation yields of different species are very low, we can either use high intensity light sources, but at the risk of damaging the sample, or time accumulative experiments. We prefer the second option, where the existence of a certain product in a given solution proves the photoactivation of oxygen, because the chemical reaction generating such a product can only occur whenever oxygen is excited to its singlet state. It is important to notice that the time scale of this chemical reaction is expected to be faster than the radiative decay rate of singlet O_2, even with the enhancement provided by the metallic nanostructure. Specifically, the following test reactions would be of interest to prove the concept (see the ESI†): (i) ''ene'' reactions to give allylic hydroperoxides, (ii) dioxetane formation through [2+2] cycloadditions and (iii) [4+2] cycloadditions to diene systems. The results (reactivity, chemo-, regio- and stereoselectivity) could be compared with those obtained using organic dyes as photosensitizers. An appropriate system to examine singlet oxygen-mediated photoadditions could be the trapping of this species by anthracene derivatives such as (1) in Fig. 4. Thus, [4+2] cycloaddition of $^1O_2$ to the central anthracene ring would afford an endoperoxide. Depending on the substitution, this endoperoxide (2) could be directly detected or can rearrange with cleavage of the 9- and/or 10-substituent to afford anthraquinone (3), as depicted in Fig. 4. The photoreaction could, in principle, be monitored by UV absorption spectroscopy, following the decrease of the characteristic long-wavelength bands of the anthracene chromophore.[87]

Conclusions

In summary, we have reported on the near-field magnetic response of different gold nanostructures and investigated their potential application for the enhancement of photochemical processes involving singlet molecular oxygen. In particular, we have focused on the magnetic dipole transitions connecting the triplet $^3\Sigma_g$ and singlet $^1\Delta_g$ states of O_2, which is a good example of dipole-forbidden transition. We have explored the response of single and tip-to-tip welded gold nanorods, which support strong dipolar plasmonic resonances involving large currents flowing along the axis of the nanostructure, and therefore produce strong magnetic fields in their vicinity. These nanoparticles have been designed for providing maximum response when used in liquid suspensions, where customarily photochemical reactions take place, and for which planar nanostructures are not suitable. Upon rigorous solution of Maxwell's equations, we have shown that the studied nanostructures display large magnetic field enhancement factors over significant volumes around them, which enhance both absorption and the emission transitions involving single oxygen. We have also provided a discussion of potential chemical reactions that could be used to detect and monitor the formation of singlet oxygen. The results of this work serve to shed light on the use of plasmonic nanostructures to realize forbidden photochemistry.

Conflicts of interest

There are no conflicts to declare.

Acknowledgements

A. M. acknowledge support from U. S. National Science Foundation (Grant ECCS-1710697). The authors acknowledge the financial support from the following projects: CTQ2014-61671-EXP, MAT2015-69669-P, and PrometeoII/2017/026. We would also like to acknowledge the UNM Center for Advanced Research Computing (CARC) for the computational resources used in this work.

References

1 N. Turro; V. Ramamurthy and J. Scaiano, *Principles of Molecular Photochemistry: An Introduction*, University Science Books, 2009.
2 L. D. Barron and C. G. Gray, The multipole interaction Hamiltonian for time dependent fields, *J. Phys. A: Math., Nucl. Gen.*, 1973, **6**, 59.
3 D. Craig and T. Thirunamachandran, *Molecular Quantum Electrodynamics: An Introduction to Radiation-molecule Interactions*, Dover Books on Chemistry Series, Dover Publications, 1984.
4 S. A. Maier, *Plasmonics: Fundamentals and Applications*, Springer, New York, 2007.
5 N. J. Halas, S. Lal, W. Chang, S. Link and P. Nordlander, Plasmons in strongly coupled metallic nanostructures, *Chem. Rev.*, 2011, **111**, 3913–3961.
6 K. Kneipp, H. Kneipp, I. Itzkan, R. R. Dasari and M. S. Feld, Ultrasensitive Chemical Analysis by Raman Spectroscopy, *Chem. Rev.*, 1999, **99**, 2957–2976.
7 S. Zhang, K. Bao, N. J. Halas, H. Xu and P. Nordlander, Substrate-Induced Fano Resonances of a Plasmonic Nanocube: A Route to Increased-Sensitivity Localized Surface

Plasmon Resonance Sensors Revealed, *Nano Lett.*, 2011, **11**, 1657–1663.

8 R. Zhang, Y. Zhang, Z. C. Dong, S. Jiang, C. Zhang, L. G. Chen, L. Zhang, Y. Liao, J. Aizpurua, Y. Luo, J. L. Yang and J. G. Hou, Chemical mapping of a single molecule by plasmon-enhanced Raman scattering, *Nature*, 2013, **498**, 82–86.

9 W. Bai, Q. Gan, F. Bartoli, J. Zhang, L. Cai, Y. Huang and G. Song, Design of plasmonic back structures for efficiency enhancement of thin-film amorphous Si solar cells, *Opt. Lett.*, 2009, **34**, 3725–3727.

10 H. A. Atwater and A. Polman, Plasmonics for improved photovoltaic devices, *Nat. Mater.*, 2010, **9**, 205–213.

11 S. Mubeen, J. Lee, W.-R. Lee, N. Singh, G. D. Stucky and M. Moskovits, On the Plasmonic Photovoltaic, *ACS Nano*, 2014, **8**, 6066–6073.

12 P. V. Kamat, Meeting the Clean Energy Demand: Nanostructure Architectures for Solar Energy Conversion, *J. Phys. Chem. C*, 2007, **111**, 2834–2860.

13 S. Linic, P. Christopher and D. B. Ingram, Plasmonic-Metal Nanostructures for Efficient Conversion of Solar to Chemical Energy, *Nat. Mater.*, 2011, **10**, 911–921.

14 W. Hou and S. B. Cronin, A Review of Surface Plasmon Resonance-Enhanced Photocatalysis, *Adv. Funct. Mater.*, 2013, **23**, 1612–1619.

15 S. Linden, C. Enkrich, M. Wegener, J. Zhou, T. Koschny and C. M. Soukoulis, Magnetic Response of Metamaterials at 100 Terahertz, *Science*, 2004, **306**, 1351–1353.

16 C. Enkrich, M. Wegener, S. Linden, S. Burger, L. Zschiedrich, F. Schmidt, J. F. Zhou, T. Koschny and C. M. Soukoulis, Magnetic metamaterials at telecommunication and visible frequencies, *Phys. Rev. Lett.*, 2005, **95**, 203901.

17 R. Merlin, Metamaterials and the Landau-Lifshitz permeability argument: Large permittivity begets high-frequency magnetism, *Proc. Natl. Acad. Sci. U. S. A.*, 2009, **106**, 1693–1698.

18 F. Monticone and A. Alu, The quest for optical magnetism: from split-ring resonators to plasmonic nanoparticles and nanoclusters, *J. Mater. Chem. C*, 2014, **2**, 9059–9072.

19 R. Verre, Z. J. Yang, T. Shegai and M. Käll, Optical Magnetism and Plasmonic Fano Resonances in Metal-Insulator-Metal Oligomers, *Nano Lett.*, 2015, **15**, 1952–1958.

20 R. A. Shelby, D. R. Smith and S. Schultz, Experimental verification of a negative index of refraction, *Science*, 2001, **292**, 77–79.

21 D. R. Smith, J. B. Pendry and M. C. K. Wiltshire, Metamaterials and negative refractive index, *Science*, 2004, **305**, 788–792.

22 C. M. Soukoulis, M. Kafesaki and E. N. Economou, Negative-Index Materials: New Frontiers in Optics, *Adv. Mater.*, 2006, **18**, 1941–1952.

23 X. Zhang and Z. Liu, Superlenses to overcome the diffraction limit, *Nat. Mater.*, 2008, **7**, 435–441.

24 D. Schurig, J. J. Mock, B. J. Justice, S. A. Cummer, J. B. Pendry, A. F. Starr and D. R. Smith, Metamaterial electromagnetic cloak at microwave frequencies, *Science*, 2006, **314**, 977–980.

25 C. Enkrich, F. Pérez-Willard, D. Gerthsen, J. Zhou, T. Koschny, C. Soukoulis, M. Wegener and S. Linden, Focused-Ion-Beam Nanofabrication of Near-Infrared Magnetic Metamaterials, *Adv. Mater.*, 2005, **17**, 2547–2549.

26 A. N. Grigorenko, A. K. Geim, H. F. Gleeson, Y. Zhang, A. A. Firsov, I. Y. Khrushchev and J. Petrovic, Nanofabricated media with negative permeability at visible frequencies, *Nature*, 2005, **438**, 335–338.

27 N. Liu, H. Guo, L. Fu, S. Kaiser, H. Schweizer and H. Giessen, Plasmon Hybridization in Stacked Cut-Wire Metamaterials, *Adv. Mater.*, 2007, **19**, 3628–3632.

28 N. I. Zheludev, The road ahead for metamaterials, *Science*, 2010, **328**, 582–583.

29 L. M. Liz-Marzán, M. Giersig and P. Mulvaney, Synthesis of Nanosized Gold-Silica Core-Shell Particles, *Langmuir*, 1996, **12**, 4329–4335.

30 L. M. Liz-Marzán, Tailoring surface plasmon through the morphology and assembly of metal nanoparticles, *Langmuir*, 2006, **22**, 32–41.

31 A. M. Funston, C. Novo, T. J. Davis and P. Mulvaney, Plasmon Coupling of Gold Nanorods at Short Distances and in Different Geometries, *Nano Lett.*, 2009, **9**, 1651–1658.

32 J. A. Fan, C. H. Wu, K. Bao, J. M. Bao, R. Bardhan, N. J. Halas, V. N. Manoharan, P. Nordlander, G. Shvets and F. Capasso, Self-Assembled Plasmonic Nanoparticle Clusters, *Science*, 2010, **328**, 1135–1138.

33 S. Linden, C. Enkrich, G. Dolling, M. W. Klein, J. Zhou, T. Koschny, C. M. Soukoulis, S. Burger, F. Schmidt and M. Wegener, Photonic Metamaterials: Magnetism at Optical Frequencies, *IEEE J. Sel. Top. Quantum Electron.*, 2006, **12**, 1097–1105.

34 M. Husnik, M. W. Klein, N. Feth, M. Konig, J. Niegemann, K. Busch, S. Linden and M. Wegener, Absolute extinction cross-section of individual magnetic split-ring resonators, *Nat. Photonics*, 2008, **2**, 614–617.

35 G. Boudarham, N. Feth, V. Myroshnychenko, S. Linden, J. Garca de Abajo, M. Wegener and M. Kociak, Spectral Imaging of Individual Split-Ring Resonators, *Phys. Rev. Lett.*, 2010, **105**, 255501.

36 P. Banzer, U. Peschel, S. Quabis and G. Leuchs, On the experimental investigation of the electric and magnetic response of a single nano-structure, *Opt. Express*, 2010, **18**, 10905–10923.

37 B.-I. Popa and S. A. Cummer, Compact Dielectric Particles as a Building Block for Low-Loss Magnetic Metamaterials, *Phys. Rev. Lett.*, 2008, **100**, 207401.

38 Q. Zhao, J. Zhou, F. Zhang and D. Lippens, Mie resonance-based dielectric metamaterials, *Mater. Today*, 2009, **12**, 60–69.

39 L. Shi, T. U. Tuzer, R. Fenollosa and F. Meseguer, A New Dielectric Metamaterial Building Block with a Strong Magnetic Response in the Sub-1.5-Micrometer Region: Silicon Colloid Nanocavities, *Adv. Mater.*, 2012, **24**, 5934–5938.

40 A. I. Kuznetsov, A. E. Miroshnichenko, Y. H. Fu, J. Zhang and B. Luk'yanchuk, Magnetic light, *Sci. Rep.*, 2012, **2**, 492.

41 A. B. Evlyukhin, S. M. Novikov, U. Zywietz, R. L. Eriksen, C. Reinhardt, S. I. Bozhevolnyi and B. N. Chichkov,

Demonstration of Magnetic Dipole Resonances of Dielectric Nanospheres in the Visible Region, *Nano Lett.*, 2012, **12**, 3749–3755.

42 B. Rolly, B. Bebey, S. Bidault, B. Stout and N. Bonod, Promoting magnetic dipolar transition in trivalent lanthanide ions with lossless Mie resonances, *Phys. Rev. B: Condens. Matter Mater. Phys.*, 2012, **85**, 245432.

43 P. Albella, M. A. Poyli, M. K. Schmidt, S. A. Maier, F. Moreno, J. J. Sáenz and J. Aizpurua, Low-Loss Electric and Magnetic Field-Enhanced Spectroscopy with Subwavelength Silicon Dimers, *J. Phys. Chem. C*, 2013, **117**, 13573–13584.

44 D. G. Baranov, R. S. Savelev, S. V. Li, A. E. Krasnok and A. Alù, Modifying magnetic dipole spontaneous emission with nanophotonic structures, *Laser Photonics Rev.*, 2017, **11**, 1600268.

45 T. Feng, Y. Zhou, D. Liu and J. Li, Controlling magnetic dipole transition with magnetic plasmonic structures, *Opt. Lett.*, 2011, **36**, 2369–2371.

46 S. M. Hein and H. Giessen, Tailoring Magnetic Dipole Emission with Plasmonic Split-Ring Resonators, *Phys. Rev. Lett.*, 2013, **111**, 026803.

47 M. Mivelle, T. Grosjean, G. W. Burr, U. C. Fischer and M. F. Garcia-Parajo, Strong Modification of Magnetic Dipole Emission through Diabolo Nanoantennas, *ACS Photonics*, 2015, **2**, 1071–1076.

48 G. S. Ofelt, Intensities of Crystal Spectra of Rare-Earth Ions, *J. Chem. Phys.*, 1962, **37**, 511–520.

49 B. R. Judd, Optical Absorption Intensities of Rare-Earth Ions, *Phys. Rev.*, 1962, **127**, 750–761.

50 C. M. Dodson and R. Zia, Magnetic dipole and electric quadrupole transitions in the trivalent lanthanide series: Calculated emission rates and oscillator strengths, *Phys. Rev. B: Condens. Matter Mater. Phys.*, 2012, **86**, 125102.

51 N. Noginova, Y. Barnakov, H. Li and M. A. Noginov, Effect of metallic surface on electric dipole and magnetic dipole emission transitions in Eu^{3+} doped polymeric film, *Opt. Express*, 2009, **17**, 10767–10772.

52 S. Karaveli and R. Zia, Spectral tuning by selective enhancement of electric and magnetic dipole emission, *Phys. Rev. Lett.*, 2011, **106**, 193004.

53 T. H. Taminiau, S. Karaveli, N. F. van Hulst and R. Zia, Quantifying the magnetic nature of light emission, *Nat. Commun.*, 2012, **3**, 979.

54 S. Karaveli, A. J. Weinstein and R. Zia, Direct Modulation of Lanthanide Emission at Sub-Lifetime Scales, *Nano Lett.*, 2013, **13**, 2264–2269.

55 N. Noginova, R. Hussain, M. A. Noginov, J. Vella and A. Urbas, Modification of electric and magnetic dipole emission in anisotropic plasmonic systems, *Opt. Express*, 2013, **21**, 23087–23096.

56 R. Hussain, D. Keene, N. Noginova and M. Durach, Spontaneous emission of electric and magnetic dipoles in the vicinity of thin and thick metal, *Opt. Express*, 2014, **22**, 7744–7755.

57 L. Aigouy, A. Cazé, P. Gredin, M. Mortier and R. Carminati, Mapping and Quantifying Electric and Magnetic Dipole Luminescence at the Nanoscale, *Phys. Rev. Lett.*, 2014, **113**, 076101.

58 R. Hussain, S. S. Kruk, C. E. Bonner, M. A. Noginov, I. Staude, Y. S. Kivshar, N. Noginova and D. N. Neshev, Enhancing Eu3+ magnetic dipole emission by resonant plasmonic nanostructures, *Opt. Lett.*, 2015, **40**, 1659–1662.

59 B. Choi, M. Iwanaga, Y. Sugimoto, K. Sakoda and H. T. Miyazaki, Selective Plasmonic Enhancement of Electric- and Magnetic-Dipole Radiations of Er Ions, *Nano Lett.*, 2016, **16**, 5191–5196.

60 R. A. Álvarez-Puebla, L. M. Liz-Marzán and F. J. Garca de Abajo, Light concentration at the nanometer scale, *J. Phys. Chem. Lett.*, 2010, **1**, 2428–2434.

61 M. Kasperczyk, S. Person, D. Ananias, L. D. Carlos and L. Novotny, Excitation of Magnetic Dipole Transitions at Optical Frequencies, *Phys. Rev. Lett.*, 2015, **114**, 163903.

62 R. Filter, S. Mühlig, T. Eichelkraut, C. Rockstuhl and F. Lederer, Controlling the dynamics of quantum mechanical systems sustaining dipole-forbidden transitions *via* optical nanoantennas, *Phys. Rev. B: Condens. Matter Mater. Phys.*, 2012, **86**, 035404.

63 A. M. Kern and O. J. F. Martin, Strong enhancement of forbidden atomic transitions using plasmonic nanostructures, *Phys. Rev. A: At., Mol., Opt. Phys.*, 2012, **85**, 022501.

64 V. Yannopapas and E. Paspalakis, Giant enhancement of dipole-forbidden transitions *via* lattices of plasmonic nanoparticles, *J. Mod. Opt.*, 2015, **62**, 1435–1441.

65 A. Alabastri, X. Yang, A. Manjavacas, H. O. Everitt and P. Nordlander, Extraordinary Light-Induced Local Angular Momentum near Metallic Nanoparticles, *ACS Nano*, 2016, **10**, 4835–4846.

66 N. Rivera, I. Kaminer, B. Zhen, J. D. Joannopoulos and M. Soljačić, Shrinking light to allow forbidden transitions on the atomic scale, *Science*, 2016, **353**, 263–269.

67 C. Schweitzer and R. Schmidt, Physical Mechanisms of Generation and Deactivation of Singlet Oxygen, *Chem. Rev.*, 2003, **103**, 1685–1758.

68 G. Herzberg, *Molecular spectra and molecular structure. Vol. 1: Spectra of diatomic molecules*, Van Nostrand Reinhold, New York, 1950, 2nd edn, 1950.

69 P. R. Ogilby, Singlet oxygen: there is indeed something new under the sun, *Chem. Soc. Rev.*, 2010, **39**, 3181–3209.

70 A. A. Ghogare and A. Greer, Using Singlet Oxygen to Synthesize Natural Products and Drugs, *Chem. Rev.*, 2016, **116**, 9994–10034.

71 M. C. De Rosa and R. J. Crutchley, Photosensitized singlet oxygen and its applications, *Coord. Chem. Rev.*, 2002, **233**, 351–371.

72 H. Kautsky and H. de Bruijn, Die Aufklärung der Photolumineszenztilgung fluorescierender Systeme durch Sauerstoff: Die Bildung aktiver, diffusionsfähiger Sauerstoffmoleküle durch Sensibilisierung, *Sci. Nat.*, 1931, **19**, 1043.

73 C. S. Foote and S. Wexler, Olefin Oxidations with Excited Singlet Molecular Oxygen, *J. Am. Chem. Soc.*, 1964, **86**, 3879–3880.

74 T. Grosjean, M. Mivelle, F. I. Baida, G. W. Burr and U. C. Fischer, Diabolo Nanoantenna for Enhancing and Confining the Magnetic Optical Field, *Nano Lett.*, 2011, **11**, 1009–1013.

75 G. González-Rubio, J. González-Izquierdo, L. Bañares, G. Tardajos, A. Rivera, T. Altantzis, S. Bals, O. Peña Rodríguez, A. Guerrero-Martínez and L. M. Liz-Marzán, Femtosecond Laser-Controlled Tip-to-Tip Assembly and Welding of Gold Nanorods, *Nano Lett.*, 2015, **15**, 8282–8288.

76 R. Toftegaard, J. Arnbjerg, K. Daasbjerg, P. Ogilby, A. Dmitriev, D. Sutherland and L. Poulsen, Metal-Enhanced 1270 nm Singlet Oxygen Phosphorescence, *Angew. Chem., Int. Ed.*, 2008, **47**, 6025–6027.

77 J. M. Wylie and J. E. Sipe, Quantum electrodynamics near an interface, *Phys. Rev. A: At., Mol., Opt. Phys.*, 1984, **30**, 1185–1193.

78 R. Carminati, J.-J. Greffet, C. Henkel and J. Vigoureux, Radiative and non-radiative decay of a single molecule close to a metallic nanoparticle, *Opt. Commun.*, 2006, **261**, 368–375.

79 L. Novotny and B. Hecht, *Principles of Nano-Optics*, Cambridge University Press, New York, 2006.

80 F. J. Garca de Abajo and A. Howie, Relativistic electron energy loss and electron-induced photon emission in inhomogeneous dielectrics, *Phys. Rev. Lett.*, 1998, **80**, 5180–5183.

81 F. J. Garca de Abajo and A. Howie, Retarded field calculation of electron energy loss in inhomogeneous dielectrics, *Phys. Rev. B: Condens. Matter Mater. Phys.*, 2002, **65**, 115418.

82 P. B. Johnson and R. W. Christy, Optical constants of the noble metals, *Phys. Rev. B: Solid State*, 1972, **6**, 4370–4379.

83 J. Gao, C. M. Bender and C. J. Murphy, Dependence of the Gold Nanorod Aspect Ratio on the Nature of the Directing Surfactant in Aqueous Solution, *Langmuir*, 2003, **19**, 9065–9070.

84 L. Scarabelli, A. Sánchez-Iglesias, J. Pérez-Juste and L. M. Liz-Marzán, A "Tips and Tricks" Practical Guide to the Synthesis of Gold Nanorods, *J. Phys. Chem. Lett.*, 2015, **6**, 4270–4279.

85 D. N. Chigrin, D. Kumar, D. Cuma and G. von Plessen, Emission Quenching of Magnetic Dipole Transitions near a Metal Nanoparticle, *ACS Photonics*, 2016, **3**, 27–34.

86 A. Pohlkötter, M. Köhring, U. Willer and W. Schade, Detection of Molecular Oxygen at Low Concentrations Using Quartz Enhanced Photoacoustic Spectroscopy, *Sensors*, 2010, **10**, 8466–8477.

87 S. J. Chadwick, D. Salah, P. M. Livesey, M. Brust and M. Volk, Singlet Oxygen Generation by Laser Irradiation of Gold Nanoparticles, *J. Phys. Chem. C*, 2016, **120**, 10647–10657.

Supporting information for:
Magnetic Light and Forbidden Photochemistry: The Case of Singlet Oxygen

Alejandro Manjavacas,*,† Roberto Fenollosa,‡ Isabelle Rodriguez,‡ M. Consuelo Jiménez,¶ Miguel A. Miranda,¶ and Francisco Meseguer*,‡

†*Department of Physics and Astronomy, University of New Mexico, Albuquerque, New Mexico 87131, United States*

‡*Instituto de Tecnología Química (CSIC - UPV), Universitat Politècnica de Valencia, Av. Tarongers s/n 46022, Valencia, Spain*

¶*Departamento de Química, Universitat Politècnica de Valencia, Av. Tarongers s/n 46022, Valencia, Spain*

E-mail: manjavacas@unm.edu; fmese@fis.upv.es

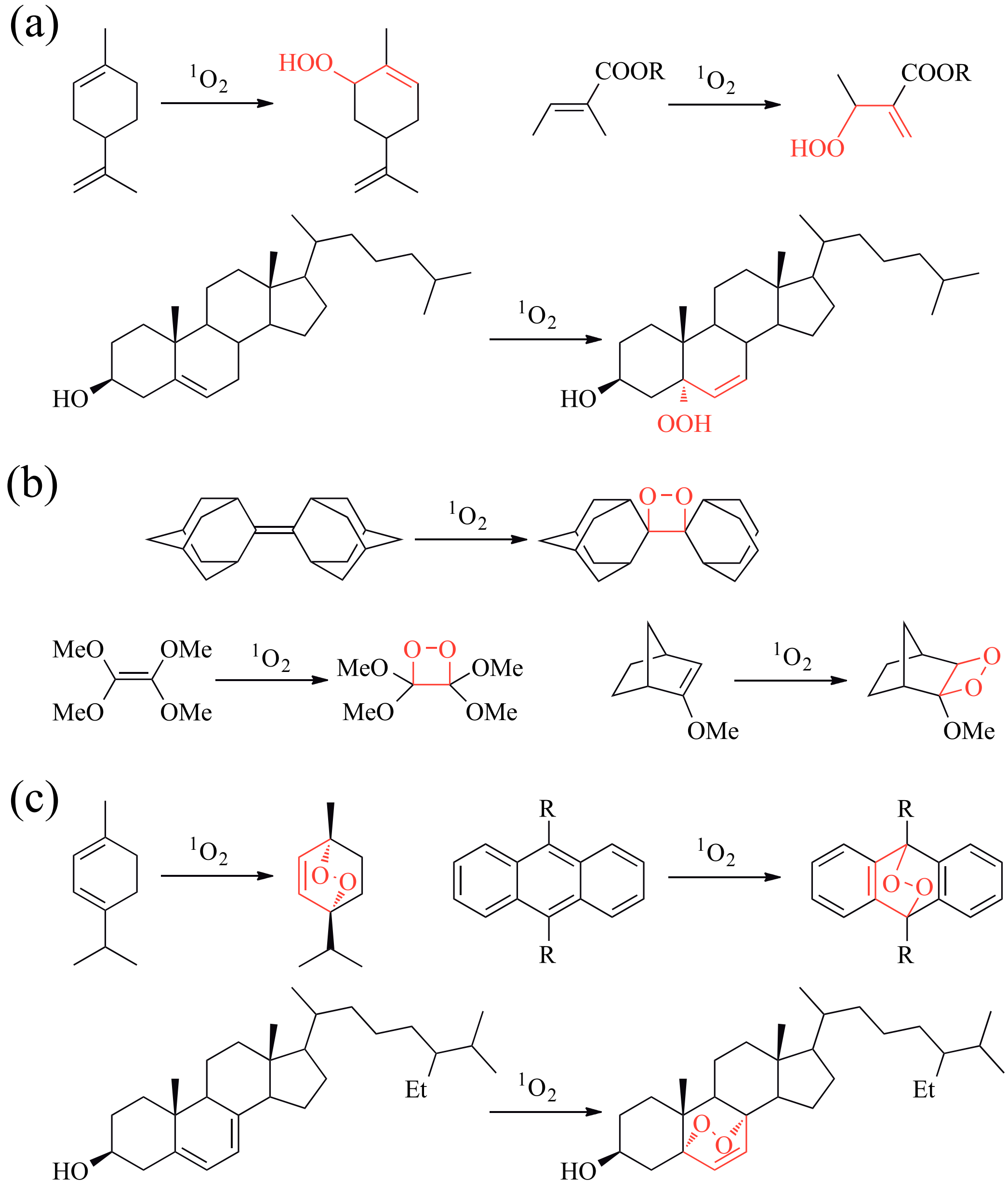

Figure S1: Test reactions of interest involving singlet oxygen that can be used for detecting and monitoring the singlet oxygen formation. (a) "ene" reactions to give allylic hydroperoxides, such as the oxygenation of limonene, tiglic acid, cholesterol. (b) Dioxetane formation through [2+2] cycloadditions with adamantylideneadamantane, tetramethoxyethene,or norbornene derivatives as probes. (c) [4+2] cycloadditions to the diene systems of 2,5-dimethylfuran, alpha-pinene, ergosterol or 9,10-disubstituted anthracenes, affording endoperoxides.